Optimization of Al^{3+} Doping on the Microstructure and Electrochemical Performance of Spinel $LiMn_2O_4$①

XIE Tao-Xiong REN Peng-Wen YU Lin-Yu LI Wei
DENG Hao-Jie JIANG Jian-Bing②
(*College of Packaging and Material Engineering, Hunan University of Technology, Zhuzhou* 412007, *China*)

ABSTRACT A series of spinel $LiAl_xMn_{2-x}O_4$ ($x \leqslant 0.1$) cathode materials was synthesized by controlled crystallization and solid state route with micro-spherical Mn_3O_4 as the precursor. X-ray diffraction (XRD) and scanning electron microscopy (SEM) were used to analyze the crystal structure of the synthetic material and the microscopic morphology of the particles. It was found that Al^{3+} doping did not change the spinel structure of the synthesized materials, and the particles had better crystallinity. In the charge and discharge test of the synthesized materials, we found that Al^{3+} doping would slightly reduce the discharge capacity, but it could effectively improve the cyclic stability of the material. The initial capacity of $LiAl_{0.04}Mn_{1.96}O_4$ is 121.6 mAh/g. After 100 cycles at a rate of 1 C (1 C = 148 mA/g), the capacity can still reach 112.9 mAh/g, and the capacity retention rate is 96.4%. Electrochemical impedance spectroscopy (EIS) suggests that Al^{3+} doping can effectively enhance the diffusion capacity of lithium ions in the material.

Keywords: micro-spherical Mn_3O_4, cyclic stability, Al^{3+} doping, cathode materials;
DOI: 10.14102/j.cnki.0254-5861.2011-3260

1 INTRODUCTION

Lithium-ion batteries (LIBS) have attracted particular attention because of their high energy density, low self-discharge, excellent cycle performance, and long life[1]. The spinel $LiMn_2O_4$ (LMO) with a three-dimensional framework structure is an important cathode material for LIBS due to its good safety[2, 3]. However, due to the dissolution of manganese and Jahn-Teller distortion in the electrode reaction process, the migration of Li^+ and the change of the valence state of manganese cation will be impeded[4-7], so that the cyclic performance of LMO in the charging-discharge cycle is rapidly reduced, especially the stability under high temperature cycle, which limits its application range[8-10].

The physicochemical properties of LMO are largely determined by the properties of precursor. Electrolytic manganese dioxide (EMD) has been widely used as a precursor for the synthesis of LMO, but EMD contains a large amount of impurities such as Na^+ and SO_4^{2-}, which will be remained in LMO and cause a sharp increase in electrochemical resistance and irreversible capacity loss during storage[11]. Spherical Mn_3O_4 [$Mn^{2+}(Mn_2^{3+})O_4$] (*I*41/*amd*) has a similar spinel structure like EMD, so it is suitable as a precursor for LMO[12-14]. The oxygen atoms are tightly packed with Mn^{2+} ions in tetrahedral sites and Mn^{3+} ions in the octahedral sites. In order to improve the physicochemical properties of LMO, researchers conducted a lot of studies and found that the doping of metal cation with valence state and radius close to Mn^{3+} can effectively improve the crystal structure and electrochemical stability of $LiM_xMn_{2-x}O_4$ (M = Al, Mg, Co, Zn, Cr, Ni, Fe, Ti)[15-22]. Wang et al. synthesized Al-doped LMO samples by the sol-gel method. Galvanostatic charge-discharge tests showed that the Al-doped LMO samples exhibited an enhanced cycle performance. When the Al doping amount is 5%, the discharge capacity retention rate of the material at a rate of 1C is about 98.2%[23]. According to Cai et al., using absorbent cotton fiber as a carrier, a simple combustion method was used to synthesize an Al-doped LMO cathode material. It is found that the particle size and

Received 20 May 2021; accepted 30 August 2021
① This work was supported by the National Natural Science Foundation of China (51604106), Foundation of Hunan Province Department of Education (18C0492), Natural Science Foundation of Hunan Province (2019JJ40070), and the China Postdoctoral Science Foundation (2016M602428)
② Corresponding author. E-mail: jjbcsu2011@163.com

lattice parameters decrease with the increase of Al doping ratio. This phenomenon is conducive to the full contact between the electrolyte and the cathode materials and shortens the diffusion distance between Li^+ ions in the solid phase[24].

In our previous paper, we successfully synthesized a uniform micro-spherical Mn_3O_4 with high purity, good uniformity and low surface area by controlled crystallization[3]. The LMO synthesized with this material as a precursor has a lower ratio Surface area, thereby reducing the electrode-electrolyte contact area. To some extent, it inhibits the dissolution of manganese during high temperature storage and circulation[25]. On this basis, we report the influence of Al doping modification on the morphology and electrochemical performance of LMO.

2 EXPERIMENTAL

2. 1 Reagents

Micro-spherical Mn_3O_4 was synthesized by controlled crystallization method[3]. Other reagents were of analytical grade. The reagents used in the experiment are analytical grade Li_2CO_3 and analytical grade NaOH produced by Meiji Chemical.

2. 2 Apparatus

To investigate the effect of aluminum mixing on $LiAl_xMn_{2-x}O_4$ ($x \leqslant 0.1$), the $LiAl_xMn_{2-x}O_4$ ($x \leqslant 0.1$) powder was characterized by X-ray diffraction (XRD, D/Max-TtriII, Japan), and its microscopic morphology was obtained by scanning electron microscope (SEM, JEOL JSM-6360LV).

The $LiAl_xMn_{2-x}O_4$ ($x \leqslant 0.1$) active material, acetylene black and binder polyvinyl fluoride (PVDF) (8:1:1, in wt%) were ground to a uniform mixture and then dissolved in N-methyl pyrrolidone (NMP) solvent and coated on the aluminum foil. After drying for 12 hours in a vacuum furnace at 120 ℃, the positive plate with a diameter of 10 mm was made after roller pressing. Lithium foil was used as the reference electrode. In an argon-filled glove box (water and oxygen concentration below 1 ppm), coin cells (CR2032) in order from the positive pole were assembled into the diaphragm (Celgard 2340 microporous membrane) to the reference electrode, and 1 $mol \cdot L^{-1}$ $LiPF_6$ is dissolved in the solution of EC-DMC-EMC (1:1:1 volume ratio) as electrolyte.

The electrochemical performance of the battery under different current densities within the voltage range of 3.0～4.3 V was tested by the battery test system (LAND CT2001A, Land Co. China) at ambient temperature and high temperature. Electrochemical impedance spectroscopy (EIS) measurements were performed on the cell with Model 2273A Electrochemical Instruments. The amplitude of the frequency AC signal is 10 mV, and the rate ranges from 0.1 Hz to 100 KHz.

2. 3 Procedure

$LiAl_xMn_{2-x}O_4$ ($x \leqslant 0.1$) was prepared by solid state route. Micro-spherical Mn_3O_4 was prepared with $MnSO_4$ using the technology in our previous paper[3]. The synthesized micro-spherical Mn_3O_4, nano $Al(OH)_3$ and Li_2CO_3 were mixed evenly and ground thoroughly in a high-efficiency mixing device. The resulting mixture was calcined in air at 750 ℃ for 12 hours at a heating rate of 10 ℃/min. After being naturally cooled to ambient temperature, the $LiAl_xMn_{2-x}O_4$ ($x \leqslant 0.1$) powder is finally obtained.

3 RESULTS AND DISCUSSION

3. 1 Structure and morphology of $LiAl_xMn_{2-x}O_4$

Fig. 1 shows the XRD pattern of $LiMn_2O_4$ and synthetic $LiAl_xMn_{2-x}O_4$ ($x \leqslant 0.1$), respectively. All samples have eight distinct diffraction peaks in the order of (111), (311), (222), (400), (331), (511), (400) and (531), consistent with spinel $LiMn_2O_4$ (JCPDS file No. 35-0782), and no other impurity peaks appear. This indicates that aluminum in the synthetic material replaces part of manganese and occupies the 16*d* position of octahedron. The obtained samples have good crystallinity and are all pure phases. The structure of the synthesized material is the same as that of $LiMn_2O_4$ with cubic spinel structure, and the space group is *Fd*-3*m*. According to the diffraction pattern, the least-squares method is used to calculate the lattice parameters of the materials, and the results are shown in Fig. 2. With the increase of Al doping, the lattice parameter drops from 0.8241 to 0.8230 nm, which may be caused by two reasons: the radius of Al^{3+} is 0.053 nm, which is smaller than that of Mn^{3+} (0.066 nm); The Mn^{3+} in the synthetic material is partially replaced by Al^{3+}, which will increase the content of Mn^{4+} to maintain charge balance, and the ionic radius of Mn^{4+} is smaller than that of Mn^{3+}. The lattice shrinkage of $LiAl_xMn_{2-x}O_4$ ($x \leqslant 0.1$) means that the binding force between the atoms inside the spinel increases, which reduces the expansion and contraction of the lattice volume during the intercalation/de-intercalation of lithium ions.

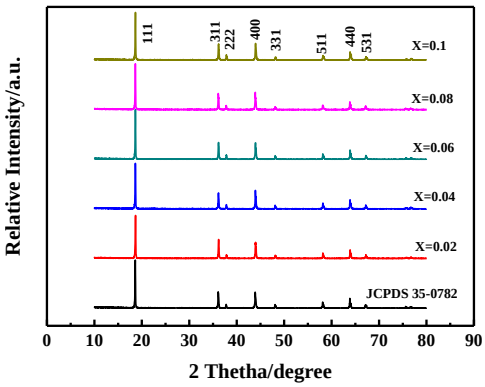

Fig. 1. XRD pattern of $LiAl_xMn_{2-x}O_4$ ($x \leqslant 0.1$)

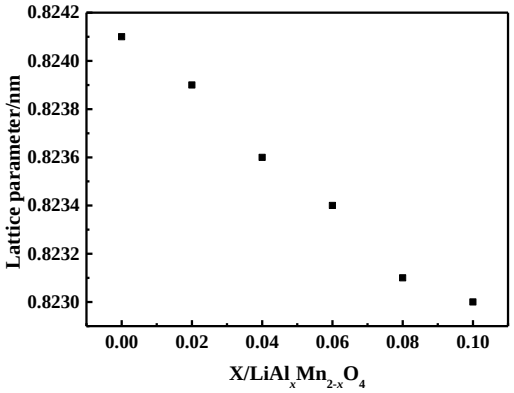

Fig. 2. XRD pattern of $LiAl_xMn_{2-x}O_4$ ($x \leqslant 0.1$)

Fig. 3 shows the SEM image of the samples. The popcorn-shaped primary particles are aggregated together to form spherical secondary particles with excellent crystal. Comparing the images with different doping contents, it can be seen that with the increase of Al doping content, the volume and particle state of the secondary particles do not change significantly, which indicates the influence of morphology and particle size on electrochemical performance can be roughly ruled out.

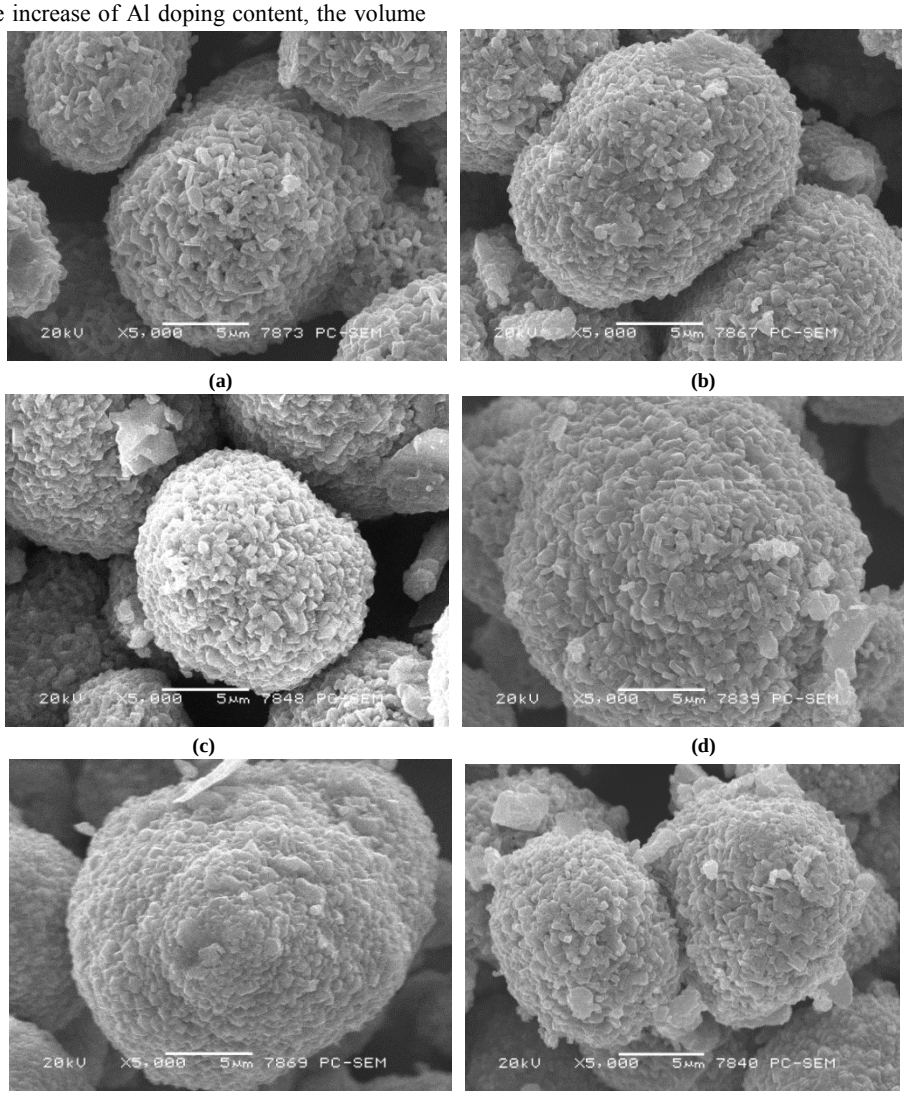

Fig. 3. SEM images of $LiAl_xMn_{2-x}O_4$: (a) x = 0, (b) x = 0.02, (c) x = 0.04, (d) x = 0.06, (e) x = 0.08, (f) x = 0.1

3. 2 Electrochemical properties of $LiAl_xMn_{2-x}O_4$

Fig. 4 compares the initial galvanostatic charge-discharge profile curves of five groups of $LiAl_xMn_{2-x}O_4$ ($x \leqslant 0.1$) and $LiMn_2O_4$ at room temperature. The voltage range is 3.0～4.3 V, and the discharge current is 0.1 C (14.8 mA/g). Obviously, all of them have two voltage platforms at 3.9 and 4.1 V, corresponding to the lithium ion intercalation/de-intercalation process. This feature is the same as spinel $LiMn_2O_4$. Table 1 shows initial galvanostatic charge-discharge capacity data of $LiAl_xMn_{2-x}O_4$ ($x \leqslant 0.1$). It can be seen from Table 1 that as Al doping increases, the charge and discharge capacity of the materials decrease. This phenomenon is caused by the decrease of active Mn^{3+} ion content[26], so considering the high specific capacity of the material, the Al doping amount will not continue to increase.

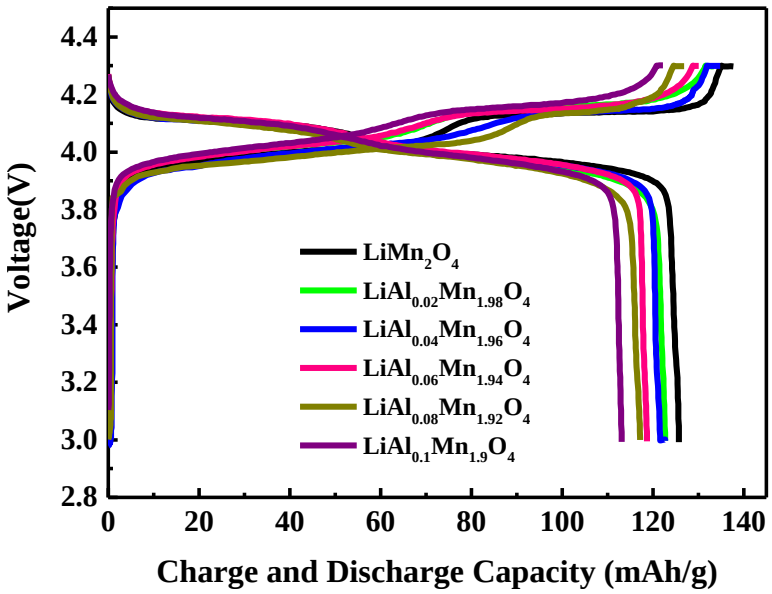

Fig. 4. Initial charge-discharge curves of $LiAl_xMn_{2-x}O_4$ ($x \leqslant 0.1$)

Table 1. Initial Charge-discharge Capacity for $LiAl_xMn_{2-x}O_4$ ($x \leqslant 0.1$)

Samples	Charge (mAh/g)	Discharge (mAh/g)
$LiMn_2O_4$	137.7	125.7
$LiAl_{0.02}Mn_{1.98}O_4$	133.4	122.7
$LiAl_{0.04}Mn_{1.96}O_4$	134.8	121.6
$LiAl_{0.06}Mn_{1.94}O_4$	130.1	118.7
$LiAl_{0.08}Mn_{1.92}O_4$	126.9	117.2
$LiAl_{0.1}Mn_{1.9}O_4$	122.3	113.1

Table 2. Discharge Capacity for $LiAl_xMn_{2-x}O_4$ ($x \leqslant 0.1$) and $LiMn_2O_4$ after 100 Cycles at Rate of 1 C at Room Temperature

Samples	Initial discharge specific capacity (mAh/g)	Discharge specific capacity after 100 cycles (mAh/g)	Capacity retention (%)
$LiMn_2O_4$	120.9	109.1	90.2
$LiAl_{0.02}Mn_{1.98}O_4$	119.1	113.5	95.3
$LiAl_{0.04}Mn_{1.96}O_4$	117.1	112.9	96.4
$LiAl_{0.06}Mn_{1.94}O_4$	116.3	110.5	95
$LiAl_{0.08}Mn_{1.92}O_4$	114.4	105.4	92.1
$LiAl_{0.1}Mn_{1.9}O_4$	111.2	100.8	90.6

Cycle stability is an important indicator that affects the application of lithium-ion batteries. Fig. 5 shows the $LiAl_xMn_{2-x}O_4$ ($x \leqslant 0.1$) and $LiMn_2O_4$ cycle performance curves between 3.0 and 4.3 V with current density of 148 mA/g (1 C~ rate) at room temperature. As can be seen from Fig. 5, the initial discharge capacity of the sample decreased slightly with the increase of the doping amount of Al because Al had no electrochemical activity[27]. As the valence of the doping element Al and the substituted element Mn was close, the capacity loss was less. $LiMn_2O_4$ has the highest initial capacity (120.9 mAh/g). After 100 cycles, the capacity decreases to 109.1 mAh/g and the capacity retention rate is 90.8%. However, with the increase of Al doping amount, the variation trend of the sample capacity retention rate was first increased and then decreased. When the doping amount x = 0.04, the material capacity retention rate reached the highest of 96.4% (from 117.1 to 112.9 mAh/g). This indicates that Al doping of $LiMn_2O_4$ can indeed improve the cyclic stability of the materials. Possible reasons for this phenomenon are: (1) Since the radius of Al^{3+} (0.053 nm) is smaller than that of Mn^{3+} (0.066 nm), the lattice parameters of Al doped materials are reduced, thus reducing the expansion and contraction of lattice volume caused by repeated insertion/detachment of lithium ions. Thus, the structural stability of spinel material is improved; (2) Al^{3+} replaces part of Mn^{3+} and the Jahn-Teller distortion is reduced accordingly.

Fig. 6 is a cycle curve diagram of pure phase $LiMn_2O_4$ and $LiAl_{0.04}Mn_{1.96}O_4$ at a charge-discharge rate of 1 C at 55 ℃. After 100 cycles, the pure phase $LiMn_2O_4$ can obtain a discharge specific capacity of 99.2 mAh/g and a capacity retention rate of 82.9%, while $LiAl_{0.04}Mn_{1.96}O_4$ can still obtain a discharge specific capacity of 104.8 mAh/g and a capacity retention rate of 89.9%. Obviously, at a higher temperature (55 ℃), $LiAl_{0.04}Mn_{1.96}O_4$ still exhibits higher cycle stability. The excellent cycle performance is due to the relatively stable crystal structure which reduces the dissolution of manganese.

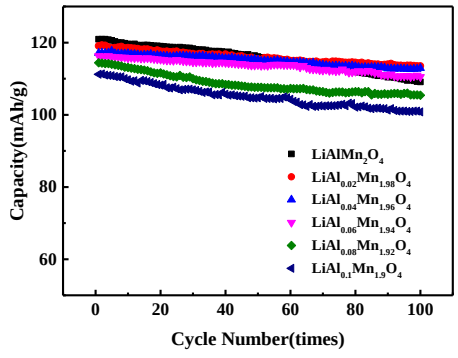

Fig. 5. Discharge cycle curves for $LiAl_xMn_{2-x}O_4$ ($x \leqslant 0.1$) and $LiMn_2O_4$ at rate of 1 C at room temperature

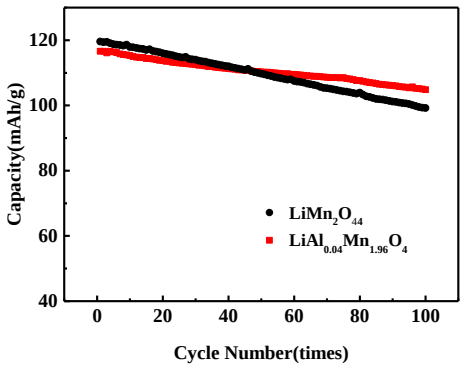

Fig. 6. Discharge cycle curves for $LiAl_{0.04}Mn_{1.96}O_4$ and $LiMn_2O_4$ at rate of 1 C at 55 ℃

Rate performance is considered to be an important index for evaluating high-power and high-energy-density lithium-ion battery cathode materials. We compared the rate performance of the pure phase $LiMn_2O_4$ and $LiAl_{0.04}Mn_{1.96}O_4$ at varying rates at room temperature. The rate performance tests of the two materials were performed in the voltage range of 3～4.3 V. Fig. 7 presents charge/discharge profiles of the pure phase $LiMn_2O_4$ and $LiAl_{0.04}Mn_{1.96}O_4$ at different current densities. Since the diffusion rate of lithium ions in the spinel structure is slow when the discharge rate is increased, the specific discharge capacity of these two materials decreases with increasing the discharge rate[28]. Fig. 8 shows the rate capability tests for the samples at different current densities. Obviously, $LiAl_{0.04}Mn_{1.96}O_4$ shows more excellent rate performance. When the discharge rate is increased to 5 C, the discharge specific capacity of $LiAl_{0.04}Mn_{1.96}O_4$ decreases to 113.3 mAh/g, which is 92.3% of the capacity at 0.1 C (122.7 mAh/g). The specific discharge capacity of $LiMn_2O_4$ is reduced to 109.2 mAh/g, which is 86.9% of the capacity (125.7 mAh/g) at 0.1 C as the smaller particle size of $LiAl_{0.04}Mn_{1.96}O_4$ has more lithium reactive sites and shorter lithium ion diffusion paths. When the rate continues to decrease from 5 to 0.1 C, the discharge specific capacity of pure phase $LiMn_2O_4$ and $LiAl_{0.04}Mn_{1.96}O_4$ can reach the initial 99.3% and 99.6%, respectively, indicating that both materials have good electrochemical reversibility.

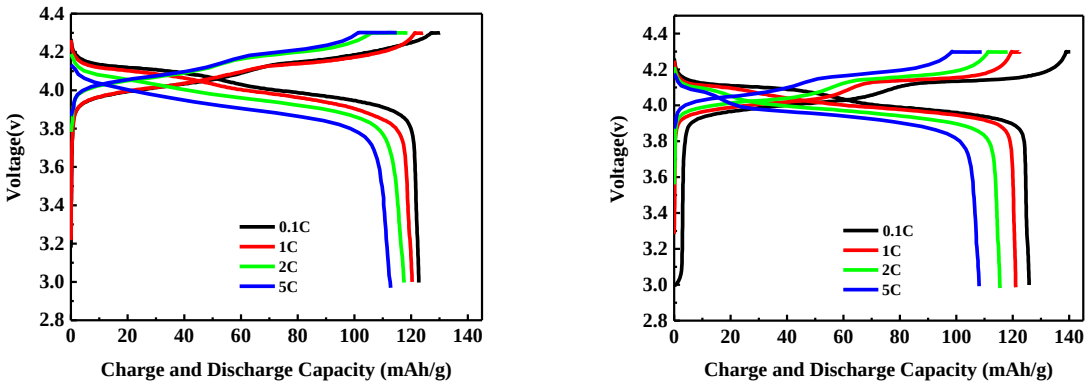

Fig. 7. Charge/discharge curve of materials at different rates: (a) $LiAl_{0.04}Mn_{1.96}O_4$, (b) $LiMn_2O_4$

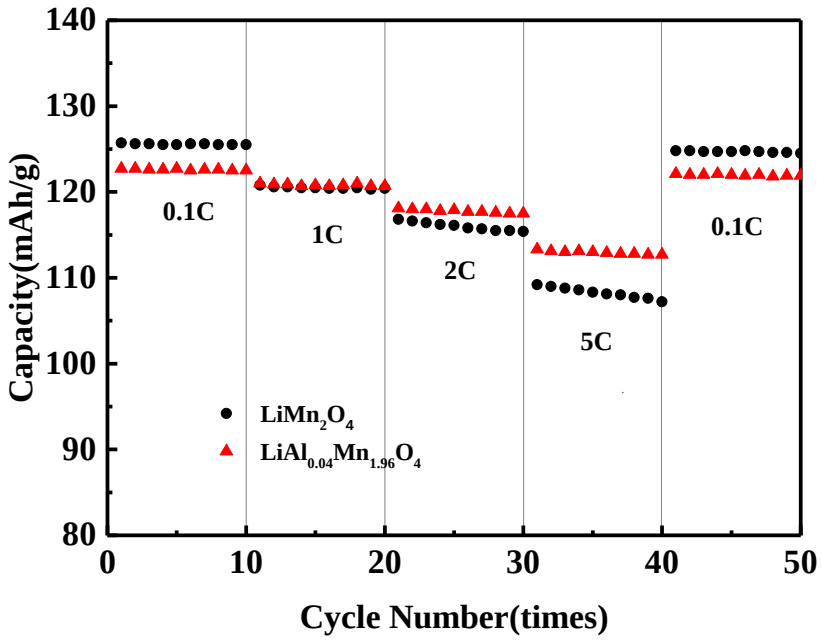

Fig. 8. Rate performance of the pure phase $LiMn_2O_4$ and $LiAl_{0.04}Mn_{1.96}O_4$ in the voltage range of 3.0~4.3 V at room temperature

The electrochemical performance of $LiMn_2O_4$ and $LiAl_{0.04}Mn_{1.96}O_4$ was compared using AC impedance spectroscopy. Fig. 9 shows the Nyquist diagram of the two materials. The equivalent simulation circuit is shown in the illustration. A semicircle in the high frequency region and a straight line in the low frequency region constitute the impedance spectrum. The high frequency area reflects the charge transfer impedance and the double layer capacitance, while the low frequency area mainly reflects the lithium ion migration impedance, which is called Warburg impedance. In the equivalent circuit, R_Ω is the Ohmic resistance of the battery, including the total resistance of electrolyte, separator, conductive material, etc.; R_{ct} represents the charge transfer resistance; CPE (Constant phase element) is used to replace the capacitor in order to fit the experimental data appropriately; CPE1 corresponds to the surface film capacitance in high-frequency semicircle; and CPE2 corresponds to double layer capacitance in the low-frequency line. The R_{ct} of $LiAl_{0.04}Mn_{1.96}O_4$ and $LiMn_2O_4$ are 41 and 869 Ω, respectively. This result shows that $LiAl_{0.04}Mn_{1.96}O_4$ is a high-quality material with lower electrochemical impedance and better electrochemical performance. This is mainly attributed to the reduction of the crystal cell volume and the shorter diffusion path of lithium ions in Al doped samples, which reduces the polarization of the material.

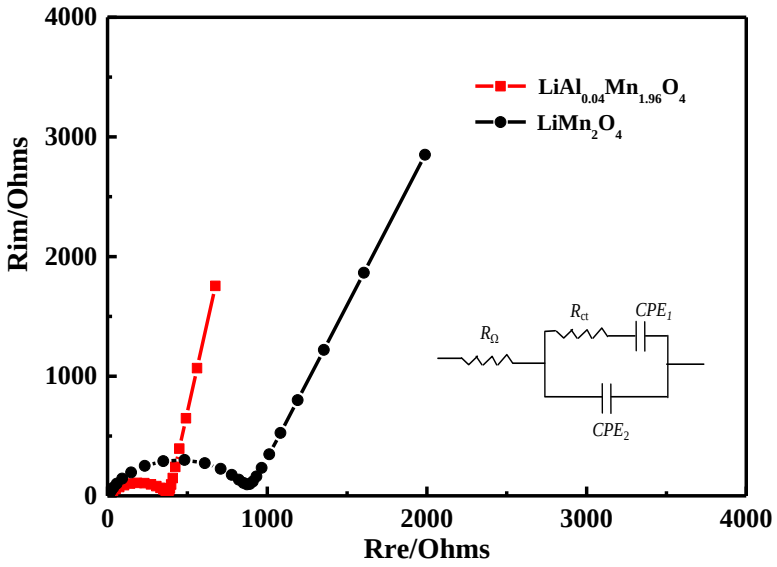

Fig. 9. Impedance spectra of pure phase $LiMn_2O_4$ and $LiAl_{0.04}Mn_{1.96}O_4$

4 CONCLUSION

We successfully synthesized $LiAl_xMn_{2-x}O_4$ ($x \leqslant 0.1$) by controlled crystallization with micro-spherical Mn_3O_4 as the precursor. XRD and SEM results show that aluminum doping enters into the spinel crystal structure, partially replaces the 16*d* manganese site, and the structure of the synthetic material is not changed. As the amount of Al doped increases, the lattice parameter of the synthesized sample decreases, and the content of active Mn^{3+} decreases, so that the initial discharge capacity of the samples decreases. But Al doping can effectively improve the cycle stability of the material. After 100 cycles at the rate of 1 C at room temperature, the initial capacity and capacity retention rate of $LiAl_{0.04}Mn_{1.96}O_4$ are 117.1 mAh/g and 96.4%, respectively, and the capacity is 113.1 mAh/g at the rate of 5 C. When the temperature rises to 55 ℃, $LiAl_{0.04}Mn_{1.96}O_4$ can still obtain a discharge specific capacity of 104.8 mAh/g and a capacity retention rate of 89.9% at the rate of 1 C, showing excellent electrochemical performance.

REFERENCES

(1) Lu, W.; Liang, L.; Sun, X.; Sun, X.; Wu, C.; Hou, L.; Sun, J.; Yuan, C. Recent progresses and development of advanced atomic layer deposition towards high-performance Li-ion batteries. *Nanomaterials* **2017**, 7, 325–28.

(2) Li, Y.; Qi, Z.; Liu, B.; Mclellan, B.; Tang, Y. Substitution effect of new-energy vehicle credit program and corporate average fuel consumption regulation for green-car subsidy. *Energy* **2018**, 152, 223–236.

(3) Jiang, J. B.; Du, K.; Cao, Y. B.; Peng, Z. D.; Hu, G. R.; Duan, J. G. Synthesis of micro-spherical Mn_3O_4 by controlled crystallization method. *Powder Technol.* **2013**, 246, 723–727.

(4) Tarascon, J. M.; Guyomard, D. The $Li_{1+x}Mn_2O_4$/C rocking-chair system: a review. *Electrochim. Acta* **1993**, 38, 1221–1231.

(5) Zhou, W. J.; Bao, S. J.; He, B. L.; Liang, Y. Y.; Li, H. L. Synthesis and electrochemical properties of $LiAl_{0.05}Mn_{1.95}O_4$ by the ultrasonic assisted rheological phase method. *Electrochim. Acta* **2006**, 51, 4701–4708.

(6) Han, C. G.; Zhu, C. Y.; Saito, G.; Akiyama, T. Improved electrochemical performance of $LiMn_2O_4$ surface-modified by a Mn^{4+}-rich phase for rechargeable lithium-ion batteries. *Electrochim. Acta* **2016**, 209, 225–234.

(7) Lin, B. H.; Yin, Q.; Hu, H. R.; Lu, F. J.; Xia, H. $LiMn_2O_4$ nanoparticles anchored on graphene nanosheets as high-performance cathode material for lithium-ion batteries. *J. Solid State Chem.* **2014**, 209, 23–28.

(8) Fergus, J. W. Recent developments in cathode materials for lithium ion batteries. *J. Power Sources* **2010**, 195, 939–954.

(9) Tron, A.; Park, Y. D.; Mun, J. Y. AlF_3-coated $LiMn_2O_4$ as cathode material for aqueous rechargeable lithium battery with improved cycling stability.

J. Power Sources **2016**, 325, 360−364.

(10) Xiao, H.; Wang, Y.; Kai, X.; Cheng, S.; Cheng, X. High capacitance $LiMn_2O_4$ microspheres with different microstructure as cathode material for aqueous asymmetric supercapacitors. *J. Alloys Compd.* **2017**, 738, 25−31.

(11) Guo, H. J.; Li, X. Q.; He, F. Y.; Li, X. H.; Wang, Z. X.; Peng, W. J. Effects of sodium substitution on properties of $LiMn_2O_4$ cathode for lithium ion batteries. *T. Nonferr. Metal. Soc.* **2010**, 20, 1043−1048.

(12) Kim, H. S.; Na, H. G.; Yang, J. C.; Jung, J. H.; Koo, Y. S.; Hur, N. J.; Kim, H. W. Annealing effects on the structure, photoluminescence, and magnetic properties of GaN/Mn_3O_4 core-shell nanowires. *J. Solid State Chem.* **2010**, 183, 2445−2450.

(13) Park, J. P.; Kim, S. K.; Park, J. Y.; Hwang, C. H.; Choi, M.; Kim, J. E.; Ok, K. M.; Kwak, H. Y.; Shim, I. W. Syntheses of Mn_3O_4 and $LiMn_2O_4$ nanoparticles by a simple sonochemical method. *Mater. Lett.* **2009**, 63, 2201−2204.

(14) Gibot, P.; Laffont, L. Hydrophilic and hydrophobic nano-sized Mn_3O_4 particles. *J. Solid State Chem.* **2007**, 180, 695−701.

(15) Fang, D. L.; Li, J. C.; Liu, X.; Huang, P. F.; Xu, T. R.; Qian, M. C.; Zheng, C. H. Synthesis of a Co–Ni doped $LiMn_2O_4$ spinel cathode material for high-power Li-ion batteries by a Sol-gel mediated solid-state route. *J. Alloys Compd.* **2015**, 640, 82−89.

(16) Kawai, H.; Nagata, M.; Tukamoto, H.; West, A. R. High-voltage lithium cathode materials. *J. Power Sources* **1999**, 81, 67−72.

(17) Zhang, H.; Liu, D.; Zhang, X. S.; Zhao, C. J.; Xu, Y. L. Microwave synthesis of $LiMg_{0.05}Mn_{1.95}O_4$ and electrochemical performance at elevated temperature for lithium-ion batteries. *J. Solid State Chem.* **2013**, 18, 569−575.

(18) Sulochana, A.; Thirunakaran, R.; Sivashanmugam, A.; Gopukumar, S.; Yamaki, J. I. Sol-gel synthesis of 5V $LiCu_xMn_{2-x}O_4$ as a cathode material for lithium rechargeable batteries. *J. Electrochem. Soc.* **2008**, 155, A206−A210.

(19) Li, Z.; Lv, X.; Wen, Y.; Fan, W.; Su, H. Carbon combustion synthesis of $LiNi_{0.5}Mn_{1.5}O_4$ and its use as a cathode material for lithium ion batteries. *J. Alloys Compd.* **2010**, 48, 802−805.

(20) Liu, G. Q.; Wen, L.; Liu, G. Y.; Tian, Y. W. Rate capability of spinel $LiCr_{0.1}Ni_{0.4}Mn_{1.5}O_4$. *J. Alloys Compd.* **2010**, 501, 233−235.

(21) Chen, M. M.; Wu, R. Y.; Ju, S. G.; Zhang, X. X.; Xue, F.; Xing, W. H. Improved performance of Al-doped $LiMn_2O_4$ ion-sieves for Li^+ adsorption. *Micropor. Mesopor. Mater.* **2018**, 261, 29−34.

(22) Zhan, D.; Liang, Y.; Cui, P.; Xiao, Z. Al-doped $LiMn_2O_4$ single crystalline nanorods with enhanced elevated-temperature electrochemical performance via a template-engaged method as a cathode material for lithiumion batteries. *RSC Adv.* **2014**, 5, 6372−6377.

(23) Wang, Y. L.; Wang, W. G; Zhang, Q.; Xin, W.; Cao, J. S.; Shi-Hai, Y. E. Electrochemical performance of Al-doped spinel $LiMn_2O_4$ cathode material for Li-ion batteries. *J. Electrochem.* **2013**, 19, 232−236.

(24) Cai, Z.; Ma, Y.; Huang, X.; Yan, X.; Yu, Z.; Zhang, S.; Song, G.; Xu, Y.; Wen, C.; Yang, W. High electrochemical stability Al-doped spinel $LiMn_2O_4$ cathode material for Li-ion batteries. *J. Energy Storage* **2020**, 27, 101036.1−101036.8.

(25) Martha, S. K.; Markevich, E.; Burgel, V.; Salitra, G.; Zinigrad, E.; Markovsky, B.; Sclar, H.; Pramovich, Z.; Heik, O.; Aurbach, D.; Exnar, I.; Buqa, H.; Drezen, T.; Semrau, G.; Schmidt, M.; Kovacheva, D.; Saliyski. N. A short review on surface chemical aspects of Li batteries: a key for a good performance. *J. Power Sources* **2009**, 189, 288−296.

(26) Han, D. W.; Ryu, W. H.; Kim, W. K.; Eom, J. Y.; Kwon, H. S. Effects of Li and Cl codoping on the electrochemical performance and structural stability of $LiMn_2O_4$ cathode materials for hybrid electric vehicle applications. *J. Phys. Chem. A* **2013**, 117, 4913−4919.

(27) Iturrondobeitia, A.; Goni, A.; Palomares, V.; Muro, I. G.; Lezama, L.; Rojo, T. Effect of doping $LiMn_2O_4$ spinel with a tetravalent species such as Si(IV) versus with a trivalent species such as Ga(III). Electrochemical, magnetic and ESR study. *J. Power Sources* **2012**, 216, 482−488.

(28) Wang, Y. Z.; Xuan, S.; Xu, H. Y.; Ming, X.; Deng, S. X.; Wang, H.; Liu, J. B.; Yan, H. Facile synthesis of porous $LiMn_2O_4$ spheres as cathode materials for high-power lithium ion batteries. *J. Power Sources* **2013**, 226, 140−148.